Mechanism and Molecular−Electronic Structure Correlations in a Novel Series of Osmium(V) Hydrazido Complexes

My Hang V. Huynh, El-Sayed El-Samanody, Konstantinos D. Demadis,[†] Peter S. White, and Thomas J. Meyer*[,‡]

Department of Chemistry, Venable and Kenan Laboratories, The University of North Carolina at Chapel Hill, Chapel Hill, North Carolina 27599-3290

Received January 14, 2000

Reaction between the Os(VI) nitrido ($Os^{VI}\equiv N^+$) complexes $[Os^{VI}(L_3)(Cl)_2(N)]^+$ (L_3 is 2,2′:6′,2″-terpyridine (tpy) or tris(1-pyrazolyl)methane (tpm)) and secondary amines ($HN(CH_2)_4O$ = morpholine, $HN(CH_2)_4CH_2$ = piperidine, and $HN(C_2H_5)_2$ = diethylamine) gives Os(V)-hydrazido complexes, $[Os^{V}(L_3)(Cl)_2(NNR_2)]^+$ (NR_2 = morpholide, piperidide, or diethylamide). They can be chemically or electrochemically oxidized to Os(VI) or reduced to Os(IV) and Os(III). The Os−N bond lengths and Os−N−N angles in the structures of these complexes are used to rationalize the bonding between the dianionic hydrazido ligand and Os. The rate law for formation of the Os(V) hydrazido complexes with morpholine as the base is first order in $[Os^{VI}(L_3)(Cl)_2(N)]^+$ and second order in $HN(CH_2)_4O$ with k_{tpy}(25 °C, CH_3CN) = (58.1 ± 1.2) M^{-2} s^{-1} and k_{tpm}(25 °C, CH_3CN) = 268.3 ± 4.0 M^{-2} s^{-1}. The proposed mechanism involves initial nucleophilic attack of the secondary amine on the Os(VI) nitrido group to give a protonated Os(IV)-hydrazido intermediate. It is subsequently deprotonated and then oxidized by $Os^{VI}\equiv N^+$ to Os(V). The extensive redox chemistry for these complexes can be explained by invoking a generalized bonding model. It can also be used to assign absorption bands that appear in the electronic from the visible−near-infrared spectra including a series of $d\pi \rightarrow d\pi$ interconfigurational bands at low energy.

Introduction

There is an emerging redox chemistry of Os(VI)-nitrido ($Os^{VI}\equiv N^+$) complexes which is extensive and has certain parallels with the reactivity of Ru(IV)-oxo complexes.[1] This includes atom transfer. An example is shown in eq 1 which results in Os(IV) phosphoraniminato complexes as products.[2]

$$\textit{trans}\text{-}[Os^{VI}(tpy)(Cl)_2(N)]^+ + PR_3 \rightarrow \textit{trans}\text{-}[Os^{IV}(tpy)(Cl)_2(NPR_3)]^+ \quad (1)$$

One-electron reduction to $Os^{V}\equiv N^0$ in dry solvents is followed by $Os^{II}(N_2)Os^{II}$ dimer formation,[3,4]

$$2\ \textit{trans}\text{-}[Os^{VI}(tpy)(Cl)_2(N)]^+ \xrightarrow{+2e^-} 2\ \textit{trans}\text{-}[Os^{V}(tpy)(Cl)_2(N)] \rightarrow \textit{trans,trans}\text{-}[(tpy)(Cl)_2Os^{II}(N_2)Os^{II}(Cl)_2(tpy)] \quad (2)$$

tpy = 2,2′:6′,2″-terpyridine

We report here an extension of this chemistry to the reactions between *trans*-$[Os^{VI}(tpy)(Cl)_2(N)]^+$ or $[Os^{VI}(tpm)(Cl)_2(N)]^+$ (tpm = tris(1-pyrazolyl)methane) and the secondary amines morpholine ($HN(CH_2)_4O$), piperidine ($HN(CH_2)_4CH_2$), or diethylamine ($HN(C_2H_5)_2$). The isolated products in these reactions are Os(V)-hydrazido complexes. We also report the existence of an extensive oxidation−reduction chemistry of the hydrazido complexes which spans oxidation states from Os(III) to Os(VI). As part of this work, we have structurally characterized examples of Os(IV), Os(V), and Os(VI) by X-ray crystallography. Part of this work has appeared in preliminary communications.[5−8]

Experimental Section

The following compounds and salts appear in this study: *trans*-$[Os^{VI}(tpy)(Cl)_2(N)](PF_6)$ **(1)**; $[Os^{VI}(tpm)(Cl)_2(N)](PF_6)$ **(2a)**; $[Os^{VI}(tpm)$-

[†] Nalco Chemical Co., Global Research, One Nalco Center, Naperville, Il 60563-1198.

[‡] Los Alamos National Laboratory, Associate Laboratory Director for Strategic and Supporting Research MS A127, Los Alamos, NM 87545. E-mail: tjmeyer@lanl.gov. Phone: 505-667-8597. Fax: 505-667-5450.

(1) (a) Naota, T.; Takaja, H.; Murahashi, S.-I. *Chem. Rev.* **1998**, *98*, 2599. (b) Carter, P. J.; Cheng, C.-C.; Thorp, H. H. *Inorg. Chem.* **1996**, *35*, 3348. (c) Dolphin, D.; Traylor, T. G.; Xie, L. Y. *Acc. Chem. Res.* **1997**, *30*, 251. (d) Liu, C. J.; Yu, W. Y.; Peng, S. M.; Mak, T. C. W.; Che, C. M. *J. Chem. Soc., Dalton Trans.* **1998**, *11*, 1805. (e) Fung, W. H.; Yu, W. Y.; Che, C. M. *J. Org. Chem.* **1998**, *63*, 3(9), 2873. (f) Muller, J. G.; Acquaye, J. H.; Takeuchi, K. J. *Inorg. Chem.* **1992**, *31*, 4552. (g) Lai, T. S.; Zhang, R.; Cheung, K. K.; Kwong, H. L.; Che, C. M. *Chem. Commun.* **1998**, *15*, 1583. (h) Bennett, S.; Brown, S. M.; Conole, G.; Kessler, M.; Rowling, S.; Sinn, E.; Woodward, S. *J. Chem. Soc., Dalton Trans.* **1995**, 368. (i) Thomsen, D. S.; Schiott, B.; Jorgensen, K. A. *J. Chem. Soc., Chem. Commun.* **1992**, 1072. (j) Che, C. M.; Yam, V. W. W. *Adv. Inorg. Chem.* **1992**, *39*, 233.

(2) (a) Demadis, K. D.; Bakir, M.; Klesczewski, B. G.; William, D. S.; Meyer, T. J.; White, P. S. *Inorg. Chim. Acta* **1998**, *270*, 511. (b) Huynh, M. H. V.; El-Samanody, El.-S.; Demadis, K. D.; White, P. S.; Meyer, T. J. Manuscript in preparation.

(3) (a) Demadis, K. D.; Meyer, T. J.; White, P. S. *Inorg. Chem.* **1997**, *36*, 5678. (b) Demadis, K. D.; El-Samanody, El.-S.; Meyer, T. J.; White, P. S. *Inorg. Chem.* **1998**, *37*, 838. (c) Demadis, K. D.; El-Samanody, El.-S.; Coia, G. M.; Meyer, T. J. *J. Am. Chem. Soc.* **1999**, *121*, 535. (d) Demadis, K. D.; Meyer, T. J.; White, P. S. *Inorg. Chem.* **1998,** *37*, 3610−3619.

(4) (a) Ware, D. C.; Taube, H. *Inorg. Chem.* **1991**, *30*, 4605. (b) Che, C.-M.; Lam, H.-W.; Tong, W.-F.; Lai, T.-F.; Lau, T.-C. *J. Chem. Soc., Chem. Commun.* **1989**, 1883.

(5) Huynh, M. H. V.; El-Samanody, E.-S.; Demadis, K. D.; Meyer, T. J.; White, P. S. *J. Am. Chem. Soc.* **1999**, *121*, 1403.

(6) Huynh, M. H. V.; White, P. S.; Meyer, T. J. *J. Am. Chem. Soc.* **1999**, *121*, 4530.

(7) Huynh, M. H. V.; El-Samanody, E.-S.; Meyer, T. J.; White, P. S. *Inorg. Chem.* **1999**, *38*, 3760.

(8) Huynh, M. H. V.; Lee, D. G.; White, P. S.; Meyer, T. J. *J. Am. Chem. Soc.* **1999**, *121*, 10446.

10.1021/ic000058e CCC: $19.00
Published on Web 06/13/2000

$(Cl)_2(^{15}N)](PF_6)$**(2*)**; $[Os^{VI}(tpm)(Cl)_2(N)](BF_4)$ **(2b)**; *trans*-$[Os^{VI}(tpy)(Cl)_2(NN(CH_2)_4O)](PF_6)_2$ **(3)**; *trans*-$[Os^{V}(tpy)(Cl)_2(NN(CH_2)_4O)](PF_6)$ **(4)**; *cis*-$[Os^{V}(tpy)(Cl)(NCCH_3)(NN(CH_2)_4O)](PF_6)_2$ **(5)**; *trans*-$[Os^{V}(tpy)(Cl)_2(NN(CH_2)_4CH_2)](PF_6)$ **(6)**; $[Os^{V}(tpm)(Cl)_2(NN(CH_2)_4O)](PF_6)$ **(7a)**; $[Os^{V}(tpm)(Cl)_2(^{15}NN(CH_2)_4O)](PF_6)$ **(7*)**; $[Os^{V}(tpm)(Cl)_2(NN(CH_2)_4O)](BF_4)$ **(7b)**; mixture of **7a** and $[Os^{IV}(tpm)(Cl)_2(N(H)N(CH_2)_4O)](PF_6)$ **(7)**; $[Os^{V}(tpm)(Cl)_2(NN(CH_2)_4CH_2)](PF_6)$ **(8a)**; $[Os^{V}(tpm)(Cl)_2(^{15}NN(CH_2)_4CH_2)](PF_6)$ **(8*)**; $[Os^{V}(tpm)(Cl)_2(NN(CH_2)_4CH_2)](BF_4)$ **(8b)**; $[Os^{V}(tpm)(Cl)_2(NN(C_2H_5)_2)](PF_6)$ **(9a)**; $[Os^{V}(tpm)(Cl)_2(NN(C_2H_5)_2)](BF_4)$ **(9b)**.

Abbreviations used in the text include the following: tpy = 2,2′:6′,2″-terpyridine; tpm = tris(1-pyrazolyl)methane; TBAH = $[N(C_4H_9)_4](PF_6)$ = tetra-(butylammonium)hexafluorophosphate.

Materials. House-distilled water was purified with a Barnstead E-Pure deionization system. High-purity acetonitrile was used as received from Burdick & Jackson. Osmium tetraoxide (>99%) was purchased from Alfa-AESAR. Morpholine, piperidine, and diethylamine were purchased from Aldrich and used without further purification. Deuterated solvents and isotopically labeled reagents were purchased from Cambridge Isotope Laboratories and used as received. TBAH was recrystallized three times from boiling ethanol and dried under vacuum at 120° for 2 days. Common laboratory chemicals employed in the preparation of compounds were reagent grade and used without further purification.

Instrumentation and Measurements. Electronic absorption spectra were acquired by using a Hewlett-Packard model 8452A diode array UV−visible spectrophotometer in quartz cuvettes. Spectra in the near-IR region were recorded on a Cary model 14 spectrophotometer by using a matched pair of 10 mm path length quartz cell. Elemental analyses were performed by Oneida Research Services, Inc. (Whitesboro, NY) and Atlantic Microlabs (Norcross, GA).

FT-IR spectra were recorded on a Mattson Galaxy 5020 series FT-IR spectrophotometer at 4 cm^{-1} resolution interfaced with an IBM-compatible PC. IR measurements were made in KBr pellets. ^1H NMR spectra were obtained in CD_3CN recorded on a Bruker-300 Fourier transform spectrometer.

Kinetic studies by UV−visible monitoring were conducted on a Hewlett-Packard 8452A diode array spectrophotometer interfaced with an IBM-compatible PC. The measurements were made in standard quartz 1 cm path length cuvettes. All kinetic studies were performed in CH_3CN at 25.0 ± 0.1 °C with a pseudo-first-order excess of morpholine. The concentrations of the Os(VI) nitrido solutions were 6.5×10^{-7} M for *trans*-$[Os^{VI}(tpy)(Cl)_2(N)]^+$ and 1.0×10^{-7} M for $[Os^{VI}(tpm)(Cl)_2(N)]^+$. The concentration of morpholine was varied from 1.11×10^{-5} to 2.77×10^{-4} M for *trans*-$[Os^{VI}(tpy)(Cl)_2(N)]^+$ and 9.69×10^{-7} to 2.42×10^{-5} M for $[Os^{VI}(tpm)(Cl)_2(N)]^+$. The temperature of solutions during the kinetic studies was maintained to within ± 0.1 °C with use of a Lauda RM6 circulating water bath and monitored with an Omega HH-51 thermocouple probe.

Cyclic voltammetric experiments were measured with the use of a PAR model 273 potentiostat, and bulk electrolyses were performed with a PAR model 173 potentiostat/galvanostat. All measurements were conducted in a three-compartment cell in CH_3CN with 0.1 M TBAH as the supporting electrolyte. A 1.0 mm platinum working electrode was used for measurements in CH_3CN, and a glassy carbon working electrode was used for the aqueous measurements. All potentials are referenced to the saturated sodium chloride calomel electrode (SSCE, 0.236 V versus NHE) at room temperature and are uncorrected for junction potentials. In all cases, the auxiliary electrode was a platinum wire. The solution in the working compartment was deoxygenated by N_2 or argon bubbling.

Synthesis and Characterization. The following complexes and compounds were prepared by literature procedures: *trans*-$[Os^{VI}(tpy)(Cl)_2(N)](PF_6)$ **(1)**;[9] $[Os^{VI}(tpm)(Cl)_2(N)](PF_6)$ **(2a)**;[3b] $[Os^{VI}(tpm)(Cl)_2(^{15}N)](PF_6)$ **(2*)**;[3b] tris(1-pyrazolyl)methane (tpm).

trans-$[Os^{V}(tpy)(Cl)_2(NN(CH_2)_4O)](PF_6)$ **(4).** In a two-necked, round-bottom flask, salt **1** (200 mg, 0.306 mmol) was stirred in 150 mL of CH_3CN under an argon atmosphere for 15 min. A 1 equiv amount of morpholine (27 μL, 0.306 mmol) in 20 mL of CH_3CN was bubbled with argon for 5 min and added dropwise into the solution of **1** through a pressure-equalizing dropping funnel. The reaction mixture was stirred continuously under argon for 1 h. The black precipitate, *trans*,*trans*-$[(tpy)(Cl)_2Os^{II}(N_2)Os^{II}(Cl)_2(tpy)]$ that formed during stirring was filtered off through a fine frit. The brown filtrate was reduced to a small volume by rotary evaporation, and the product was obtained by recrystallization from CH_3CN/Et_2O. Yield: 0.102 g (45.1%). Anal. Calcd for $OsCl_2C_{19}H_{19}N_5OPF_6 \cdot 0.5\ H_2O$: C, 30.49; H, 2.69; N, 9.36. Found: C, 30.22; H, 2.71; N, 9.39. Infrared (cm^{-1}, KBr disk): ν(tpy) 1603 (vs), 1449 (vs), and 1245 (vs); ν(CO) 1094 (vs); $\nu(\pi$NN) 1346.

trans-**$[Os^{V}(tpy)(Cl)_2(NN(CH_2)_4CH_2)](PF_6)$ (6).** This salt was prepared by a method similar to that used for **4**. Yield: 67.6 mg (30.0%). Anal. Calcd for $OsCl_2C_{20}H_{21}N_5PF_6 \times e1 \cdot H_2O$: C, 31.80; H, 3.07; N, 9.27. Found: C, 31.61; H, 2.81; N, 9.39. Infrared (cm^{-1}, KBr disk): ν(tpy) 1601 (vs), 1450 (vs), and 1246 (vs); $\nu(\pi$NN) 1352.

trans-**$[Os^{VI}(tpy)(Cl)_2(NN(CH_2)_4O)](PF_6)_2$ (3).** *trans*-$[Os^{VI}(tpy)(Cl)_2(NN(CH_2)_4O)](PF_6)_2$ was electrochemically generated from **4** by electrolysis at E_{app} = 1.23 V (versus SSCE) in CH_3CN (0.1 M TBAH), and the resulting Os(VI) hydrazido complex was isolated by diffusion of Et_2O into the electrochemically generated solution under argon. Anal. Calcd for $OsCl_2C_{19}H_{19}N_5OP_2F_{12} \cdot CH_3CN$: C, 27.25; H, 2.40; N, 9.08. Found: C, 27.42; H, 2.67; N, 9.06.

$[Os^{V}(tpm)(Cl)_2(NN(CH_2)_4O)](PF_6)$ (7a). In a 100 mL round-bottom flask was dissolved salt **2a** (300 mg, 0.47 mmol) in 20 mL of CH_3CN. A 1 equiv amount of morpholine (41 μL, 0.47 mmol) in 20 mL of CH_3CN was added while stirring over a period of 10 min. A fine brown precipitate that formed during stirring was filtered off through a fine frit. The green filtrate was evaporated to 5 mL, and the addition of 400 mL of Et_2O caused precipitation of an olive green product. It was further purified by recrystallization from a CH_3CN/Et_2O mixture, filtered off, and air-dried. Yield: 0.150 g (44.0%). The product was a mixture of $[Os^{V}(tpm)(Cl)_2(NN(CH_2)_4O)](PF_6)$ and $[Os^{IV}(tpm)(Cl)_2(N(H)N(CH_2)_4O)](PF_6)$ which were identified by the X-ray crystallography and electrochemical measurements (see below). Anal. Calcd for $OsC_{14}H_{18}Cl_2N_8OPF_6$: C, 23.30; H, 2.52; N, 15.54. Found: C, 22.83; H, 2.85; N, 15.56. Infrared (cm^{-1}, KBr disks): ν(tpm) 1511, 1415, and 1271; ν(NN) 1218 (vs); ν(CO) 1089 (vs); ν(PF) 851 (vs).

$[Os^{V}(tpm)(Cl)_2(^{15}NN(CH_2)_4O)](PF_6)$ (7*). This salt was prepared by a method similar to that used for **7a** except that $[Os^{VI}(tpm)(Cl)_2(^{15}N)](PF_6)$ (**2***) was used as the starting material. Infrared (cm^{-1}, KBr disk): $\nu(^{15}\pi$NN) 1207.

$[Os^{V}(tpm)(Cl)_2(NN(CH_2)_4O)](BF_4) \cdot 2H_2O$ (7b). This salt was prepared by the same method as used for **7a** except that $[Os^{VI}(tpm)(Cl)_2(N)](BF_4)$ (**2b**) was used as the starting material. Anal. Calcd for $OsC_{14}H_{18}Cl_2N_8OBF_4 \cdot 2\ H_2O$: C, 24.03; H, 3.17; N, 16.02. Found: C, 23.58; H, 3.06; N, 15.66. Infrared (cm^{-1}, KBr disks): ν(tpm) 1512, 1412 and 1272; ν(NN) 1220; ν(BF) 1063.

$[Os^{V}(tpm)(Cl)_2(NN(CH_2)_4CH_2)](PF_6)$ (8a). In a 100 mL round-bottom flask was dissolved salt **2a** (300 mg, 0.47 mmol) in 20 mL of CH_3CN. A 1 equiv amount of piperidine (46 μL, 0.47 mmol) in 20 mL of CH_3CN was added while stirring over a period of 30 min. This product was isolated in a similar manner as for **7a**. Yield: 0.130 g (38.0%). Anal. Calcd for $OsC1_5H_{20}Cl_2N_8PF_6$: C, 25.03; H, 2.80; N, 15.85. Found: C, 24.70; H, 2.79; N, 15.54. Infrared (cm^{-1}, KBr disks): ν(tpm) 1515, 1411, and 1281; ν(NN) 1228 (vs); ν(PF) 845 (vs).

$[Os^{V}(tpm)(Cl)_2(^{15}NN(CH_2)_4CH_2)](PF_6)$ (8*). This salt was prepared by the same method as used for **8a** except $[Os^{VI}(tpm)(Cl)_2(^{15}N)](PF_6)$ (**2***) was used as the starting material. Infrared (cm^{-1} KBr disks): $\nu(^{14}$NN) 1224.

$[Os^{V}(tpm)(Cl)_2(NN(CH_2)_4CH_2)](BF_4) \cdot 2\ H_2O$ (8b). This salt was prepared by the same method as for **8a** except that $[Os^{VI}(tpm)(Cl)_2(N)](BF_4)$ (**2b**) was used as the starting material. Anal. Calcd for $OsC_{15}H_{20}Cl_2N_8BF_4 \cdot 2\ H_2O$: C, 25.82; H, 3.47; N, 16.07. Found: C, 25.63; H, 3.46; N, 15.89. Infrared (cm^{-1}, KBr disks): ν(tpm) 1515, 1408 and 1285; ν(NN) 1226; ν(BF) 1055.

$[Os^{V}(tpm)(Cl)_2(NN(C_2H_5)_2)](PF_6) \cdot 2\ H_2O$ (9a). In a 100 mL round-bottom flask was dissolved salt **2a** (200 mg, 0.31 mmol) in 20 mL of CH_3CN. A 1 equiv amount of diethylamine (32 μL, 0.31 mmol) in 10

(9) (a) Williams, D. S.; Coia, G. M.; Meyer, T. J. *Inorg. Chem.* **1995**, *34*, 586. (b) Pipes, D. W.; Bakir, M.; Vitols, S. E.; Hodgson, D. J.; Meyer, T. J. *J. Am. Chem. Soc.* **1990**, *112*, 5514.

Table 1. Summary of Crystal Data, Intensity Collection, and Structure Refinement Parameters for *trans*-[Os^{VI}(tpy)$(Cl)_2$($NN(CH_2)_4O$)]$(PF_6)_2$ (**3**), *cis*-[Os^{V}(tpy)(Cl)(CH_3CN)($NN(CH_2)_4O$)]$(PF_6)_2$ (**5**), *trans*-[Os^{V}(tpy)$(Cl)_2$($NN(CH_2)_4CH_2$)](PF_6) (**6**), [Os^{IV}(tpm)$(Cl)_2$($N(H)N(CH_2)_4O$)](PF_6) (**7a**), and [Os^{V}(tpm)$(Cl)_2$($NN(C_2H_5)_2$)](PF_6) (**9b**)

	Salts				
	3	**5**	**6**	**7a**	**9b**
Formula	$OsC_{19}H_{19}Cl_2N_5OP_2F_{12}$	$OsC_{21}H_{22}ClN_6OP_2F_{12}\cdot 0.5CH_3CN$	$OsC_{22}H_{24}Cl_2N_6PF_6$	$OsC_{14}H_{19}C1_2N_8OPF_6\cdot 3CH_3CN$	$OsC_{14}H_{20}Cl_2N_8BF_4$
M_r	884.42	745.07	737.493	844.58	648.27
a (Å)	9.9697(5)	11.3733(5)	14.1724(17)	14.8348(7)	9.3411(5)
b (Å)	15.4863(7)	35.4146(16	16.3483(20)	11.7758(6)	25.5779(14)
c (Å)	18.3680(8)	15.1697(7)	11.88.53(14)	17.3115(9)	10.0974(6)
γ (deg)	90	90	90	90	90
β (deg)	105.642(1)	95.813(1)	95.436(2)	93.432(1)	116.554(1)
γ (deg)	90	90	90	90	90
V (Å^3)	2730.88(22)	6078.6(5)	2741.4(6)	3018.8(3)	2158.04(21)
Z	4	8	4	4	4
cryst system	monoclinic	monoclinic	monoclinic	monoclinic	monoclinic
space group	$P2_1/n$	Cc	$P2_1/c$	$P2_1/a$	$P2_1/a$
cryst size (mm)	0.40 × 0.10 × 0.05	0.40 × 0.05 × 0.05	0.20 × 0.20 × 0.05	0.30 × 0.20 × 0.01	0.20 × 0.20 × 0.35
d_{calcd} (g/cm3)	2.15	1.990	1.886	1.856	1.995
diffractometer	Bruker Smart	Bruker Smart	Bruker Smart	Siemens Smart	Bruker Smart
radiation (λ, Å)	Mo Kα (0.710 73)	Mo Kα (0.710 73)	Mo Kα (0.710 73)	Mo Kα (0.710 73)	Mo Kα (0.710 73)
collcn temp	−100	−100	−100	−100	−100
abs. coeff μ, (cm^{-1})	0.509	0.449	0.494	0.435	0.621
F(000)	1695.93	3518.81	1507.13	1643.26	1242.53
$2\theta_{max}$ (deg)	50.0	50.0	50.0	50.0	60.0
tot. reflns	13 656	26 223	15 665	25 208	10 907
unique reflns	4821	10725	4844	5335	5838
refined reflns	3624	7689	3570	3840	4562
merging R value	0.033	0.044	0.048	0.062	0.029
no. of params	379	818	334	379	272
R (%)[a]	6.0	3.4	4.8	4.5	3.1
R_w (%)[b]	4.7	3.8	5.9	5.1	3.3
goodness of fit[c]	1.73	1.11	2.09	2.00	2.03
deepest Hole (e/Å^3)	−1.950	−1.580	−3.080	−2.800	−1.250
highest peak (e/Å^3)	1.590	1.480	3.100	2.920	1.620

[a] $R = \sum(|F_o - F_c|)\sum|F_o|$. [b] $R_w = [\sum(w|F_o - F_c|)^2/\sum w(F_o)^2]^{1/2}$. [c] GoF $= [\sum w(F_o - F_c)^2/(\text{no. of reflns} - \text{no. of params})]^{1/2}$.

mL of CH_3CN was added while stirring over a period of 30 min. This product was isolated in a similar procedure used for **7a**. Yield: 35 mg (15.0%). Anal. Calcd for $OsC_{14}H_{20}Cl_2N_8PF_6\cdot 2H_2O$: C, 22.65; H, 3.26; N, 15.09. Found: C, 22.66; H, 2.65; N, 13.99. Infrared (cm^{-1}, KBr disks): ν(tpm) 1445, 1407, and 1284; ν(NN) 1227 (vs); ν(PF) 846 (vs).

[Os^{V}(tpm)$(Cl)_2$($NN(CH_2CH_3)_2$)](BF_4) (9b). This salt was prepared by the same method as used for **9a** on a very small scale for the purpose of preparing single crystals for X-ray structure determination.

X-ray Structural Determinations. Data Collection, Solution, and Refinement of the Structures. Single crystals of **3**, **5**, **6**, and **7a** were obtained by a slow diffusion of Et_2O into a CH_3CN solution. Single crystals of **9b** were obtained by layering Et_2O onto a CH_2Cl_2 solution. Crystal data, intensity collection information, and structure refinement parameters for the structures are listed in Table 1. The structures were solved by direct methods. The remaining non-hydrogen atoms were located in subsequent difference Fourier maps. Empirical absorption corrections were applied with SADABS. The ORTEP plotting program was used to computer generate the structures shown in Figures 1−3.[10] An ORTEP diagram for [Os^{IV}(tpm)$(Cl)_2$($N(H)N(CH_2)_4O$)]$^+$ has been published although incorrectly labeled as [Os^{V}(tpm)$(Cl)_2$($NN(CH_2)_4O$)]$^+$.[5] Hydrogen atoms were included in calculated positions with thermal parameters derived from the atom to which they were bonded. All computations were performed by using the NRCVAX suite of programs.[11] Atomic scattering factors were taken from a standard source[12] and corrected for anomalous dispersion. The crystal lattice containing [Os^{IV}(tpm)$(Cl)_2$($N(H)N(CH_2)_4O$)]$^+$ also contains three molecules of acetonitrile per asymmetric unit. The crystal unit of **5** contains two Os(V) hydrazido molecules in which two molecules are distinguished from each other by an inversion center. The final positional parameters along with their standard deviations as estimates from the inverse matrix and tables of hydrogen atom parameters, anisotropic thermal parameters, and observed/calculated structure amplitudes for **3**, **5**, **6**, **7a**, and **9b** are available as Supporting Information. Selected bond distances and angles for the compounds are listed in Tables 2 and 3, respectively.

Results

Synthesis and Mechanism of Formation. In the preparations of **4** and **6**, stoichiometric addition of the secondary amine in CH_3CN (1.53×10^{-2} M) to *trans*-[Os^{VI}(tpy)$(Cl)_2$(N)](PF_6) in CH_3CN (2.04×10^{-3} M) resulted in color changes from magenta to brown on a time scale of minutes with the coformation of *trans*,*trans*-[(tpy)$(Cl)_2Os^{II}(N_2)Os^{II}(Cl)_2$(tpy)] as a black solid. After filtration, the brown solutions were reduced to a small volume, and brown solids **4** and **6** were isolated.

For **7** and **8**, the addition of HNR_2 (2.36×10^{-2} M) to equimolar [Os^{VI}(tpm)$(Cl)_2$(N)](PF_6) in CH_3CN caused the color of the solution to change from orange to green with the formation of a brown solid. For **9**, the color changed from orange to brown. The green and brown solutions were collected by filtration, and upon addition of Et_2O, the green and brown solids were separately obtained. The Os(V) complexes were characterized by X-ray crystallography, cyclic voltammetry, elemental analysis, and infrared and UV−visible spectroscopies.

The product yields of 45.1% for **4** and 44.0% for **7** are consistent with the proposed mechanism (see below) in which the formation of the μ-N_2 dimer occurs by reduction of $Os^{VI}\equiv N^+$ to $Os^{V}\equiv N^0$ followed by N···N coupling. For **7**, two products

(10) Johnson, C. K.; *ORTEP: A Fortran Thermal Ellipsoid Plot Program*; Technical Report ORNL-5138; Oak Ridge National Laboratory: Oak Ridge, TN, 1976.
(11) Gabe, E. J.; Le Page, Y.; Charland, J.-P.; Lee, F. L.; White, P. S. *J. Appl. Crystallogr.* **1989**, *22*, 384.
(12) *International Tables for X-ray Crystallography*; Kynoch Press: Birmingham, U.K.; 1974; Vol. IV.

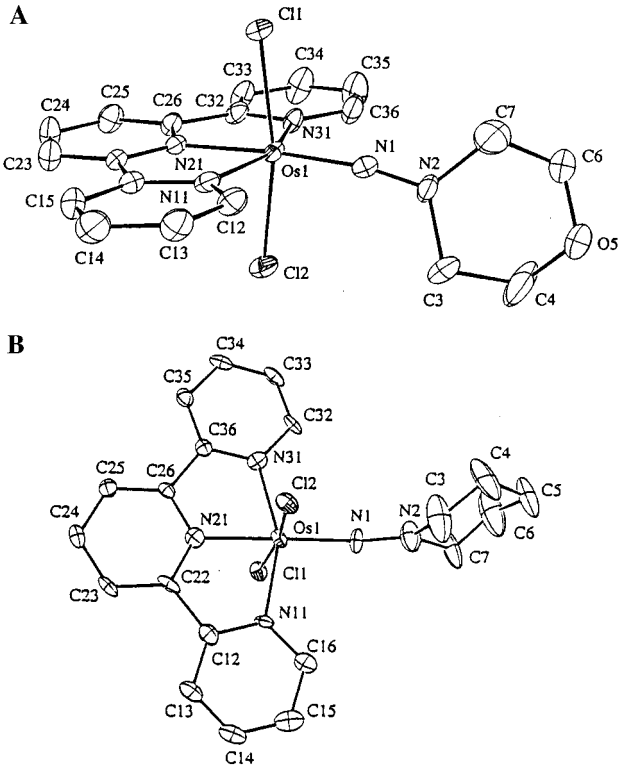

Figure 1. (A) ORTEP diagram (30% ellipsoids) and labeling scheme for the cation *trans*-$[Os^{VI}(tpy)(Cl)_2(NN(CH_2)_4O)]^{2+}$ in the PF_6^- salt. (B) ORTEP diagram (30% ellipsoids) and labeling scheme for the cation *trans*-$[Os^{V}(tpy)(Cl)_2(NN(CH_2)_4CH_2)]^{+}$ in the PF_6^- salt.

were isolated, $[Os^{V}(tpm)(Cl)_2(NN(CH_2)_4O)](PF_6)$, **7a**, and $[Os^{IV}(tpm)(Cl)_2(N(H)N(CH_2)_4O)](PF_6)$. The latter, the protonated form of Os(IV), was identified by cyclic voltammetry (Figure 4B). The details of this formation will be discussed later in the Discussion.

Reactions also occur between the Os(VI) nitrido complexes and a variety of primary and tertiary amines. These reactions are currently under investigation.

The kinetics of formation of the Os(V) products for the reactions between *trans*-$[Os^{VI}(tpy)(Cl)_2(N)](PF_6)$ or $[Os^{VI}(tpm)(Cl)_2(N)](PF_6)$ and morpholine were studied by conventional mixing and UV−visible monitoring in CH_3CN at 25.0 ± 0.1 °C. A typical kinetic trace is shown in Supplementary Figure S1. The kinetic studies were carried out under pseudo-first-order conditions with a large excess of morpholine from 1.11×10^{-5} to 2.77×10^{-4} M. As shown by the plots of k_{obs} versus $[HN(CH_2)_4O)]^2$ in Figure 5, the kinetics are second order in amine consistent with the rate law

$$\frac{-d[Os^{VI}N^+]}{dt} = k[Os^{VI}{\equiv}N^+][HN(CH_2)_4O]^2 = k_{obs}[Os^{VI}{\equiv}N^+] \quad (3)$$

with $k_{obs} = k[HNR_2]^2$. Each rate constant in Figure 5 was the average of 3 independent experiments. On the basis of the experimental slopes and eq 3, $k_{tpy} = (5.81 \pm 0.01) \times 10^1$ M^{-2} s^{-1} and $k_{tpm} = (2.68 \pm 0.04) \times 10^2$ M^{-2} s^{-1}.

Redox Chemistry and Solvolysis. All of the hydrazido compounds have extensive redox chemistries. The cyclic voltammogram of $[Os^{V}(tpm)(Cl)_2(NN(CH_2)_4O)]^+$ in CH_3CN in Figure 4B provides evidence for chemically reversible Os(VI/V), Os(V/IV), and Os(IV/III) couples on the cyclic voltammetry time scale at a scan rate of 200 mV/s. In Figure 4A is shown a

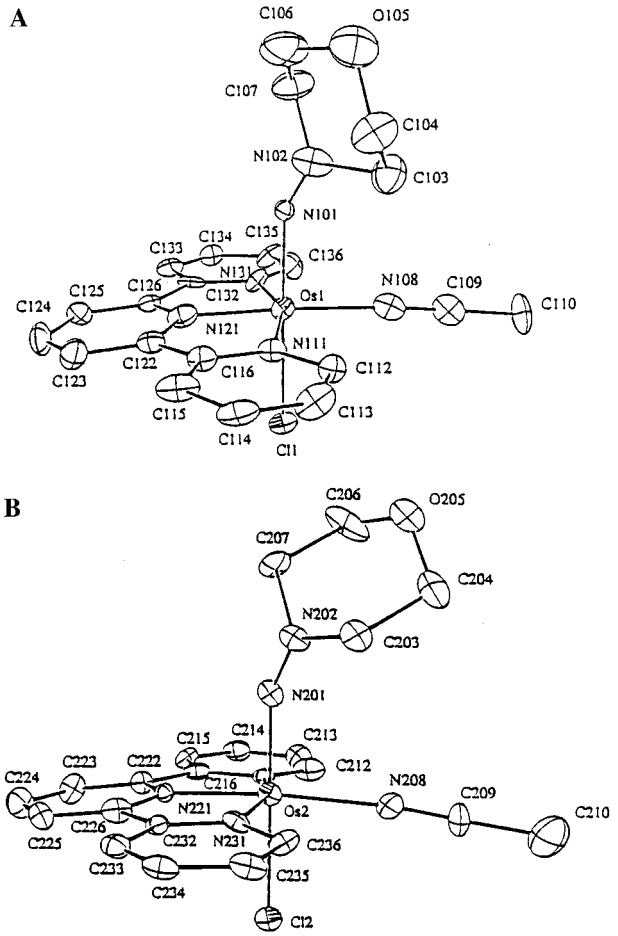

Figure 2. (A) ORTEP diagrams (30% ellipsoids) and labeling schemes for the cations *cis*-$[Os^{V}(tpy)(Cl)(CH_3CN)(NN(CH_2)_4O)]^{2+}$ in the PF_6^- salt.

cyclic voltammogram of $[Os^{IV}(tpm)(Cl)_2(N(H)N(CH_2)_4O)]^+$. Upon addition of 2,2′-bipyridine as a base, the deprotonated form of Os(V), $[Os^{V}(tpm)(Cl)_2(NN(CH_2)_4O)]^+$, appears as shown in Figure 4C. $E_{1/2}$ values from cyclic voltammetry and UV−visible spectroscopic data are listed in Table 4.

Stabilities of both the Os(VI) and Os(IV) forms were investigated by electrochemical measurements in CH_3CN. Oxidation of *trans*-$[Os^{V}(tpy)(Cl)_2(NN(CH_2)_4O)]^+$ to *trans*-$[Os^{VI}(tpy)(Cl)_2(NN(CH_2)_4O)]^{2+}$ occurs with $n = 1$ by coulometry. Cyclic voltammograms before and after oxidation were the same. UV−visible data on electrochemically generated *trans*-$[Os^{VI}(tpy)(Cl)_2(NN(CH_2)_4O)]^{2+}$ are given in Table 4.

Reduction of *trans*-$[Os^{V}(tpy)(Cl)_2(NN(CH_2)_4O)]^+$ to Os(IV) also occurs with $n = 1$, but reduction is followed by isomerization and solvolysis to form *cis*-$[Os^{IV}(tpy)(Cl)(NCCH_3)(NN(CH_2)_4O)]^+$. The details of this chemistry will be discussed in a later paper.[13] Further oxidation of the solvolysis complex at $E_{app} = 1.23$ V gives **5**, which was characterized by X-ray crystallography, cyclic voltammetry, and UV−visible spectroscopy (Table 4).

UV−Visible Spectra. UV−visible spectra for *trans*-$[Os^{VI}(tpy)(Cl)_2(NN(CH_2)_4O)]^{2+}$, *trans*-$[Os^{V}(tpy)(Cl)_2(NN(CH_2)_4O)]^+$, and *trans*-$[Os^{IV}(tpy)(Cl)_2(N(H)N(CH_2)_4O)]^+$ in CH_3CN are shown in Figure 6. The spectra are summarized in Table 4. Band assignments are given in Table 5.

(13) (a) Huynh, M. H. V.; White, P. S.; Meyer, T. J. Synthesis and Characterization of Os(IV)-Hydrazido Complexes. Work in progress. (b) Huynh, M. H. V.; Meyer, T. J. Work in progress.

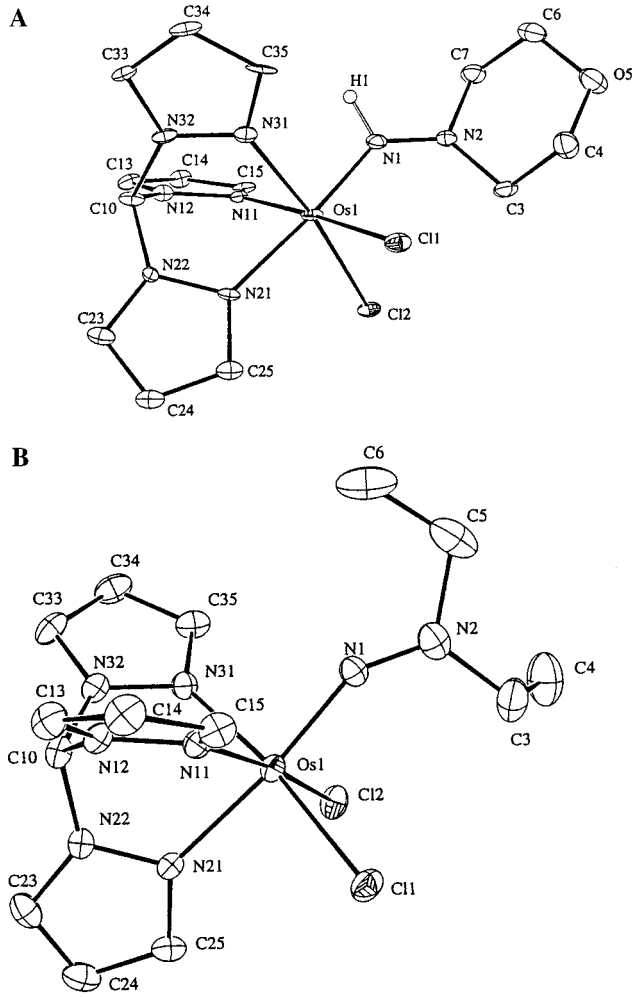

Figure 3. (A) ORTEP diagram (30% ellipsoids) and labeling scheme for the cation $[Os^{IV}(tpm)(Cl)_2(N(H)N(CH_2)_4O)]^+$ in the PF_6^- salt. (B) ORTEP diagram (30% ellipsoids) and labeling scheme for the cation in $[Os^{V}(tpm)(Cl)_2(NN(C_2H_5)_2)]^+$ as the BF_4^- salt.

For the tpm complexes ($[Os^{VI}(tpm)(Cl)_2(NN(CH_2)_4O)]^{2+}$, $[Os^{V}(tpm)(Cl)_2(NN(CH_2)_4O)]^{+}$, and $[Os^{IV}(tpm)(Cl)_2(NN(CH_2)_4O)]$), characteristic $\pi \rightarrow \pi^*$ (tpm) bands appear in the UV at 216, 272, and 314 nm for Os(VI); at 214, 228, and 326 nm for Os(V); and at 212, 274, and 318 nm for Os(IV). For **7a**, an interconfigurational (IC) $d\pi \rightarrow d\pi$ band appears at 610 nm, and a ligand-to-metal (LMCT) band appears at 382 nm. The detailed origin of these transitions for the tpy complexes will be discussed in a later section. In the spectrum of $[Os^{IV}(tpm)(Cl)_2(N(H)N(CH_2)_4O)]^+$, a metal-to-ligand (MLCT) band of high intensity appears in the visible at $\lambda_{max} = 396$ nm with $\epsilon = 1.66 \times 10^4$ M^{-1} cm^{-1} compared to $\lambda_{max} = 472$ nm and $\epsilon = 5.13 \times 10^3$ M^{-1} cm^{-1} for *trans*-$[Os^{IV}(tpy)(Cl)_2(N(H)N(CH_2)_4O)]^+$ in CH_3CN in the presence of HPF_6.

Infrared Spectra. The infrared spectra of **7a**, **8a**, **7***, and **8*** were obtained in KBr pellets. Spectra are shown in Supplementary Figure S2. In these spectra, significant differences between the ^{14}N and the ^{15}N complexes appear in the region 1200−1250 cm^{-1}. In other hydrazido complexes, ν(NN) of the hydrazido ligand appears in the range 1315−1510 cm^{-1}.[16] For **7a**, a band at ∼1218 cm^{-1} in the ^{14}N complex shifts to 1207 cm^{-1} in the ^{15}N complex. The shift of ∼11 cm^{-1} is less than the calculated 23 cm^{-1} by Hook's law approximation. This suggests that this band is a mixed mode with appreciable ν(NN) character. For **8a**, the shift is even smaller with bands appearing at 1228 cm^{-1} for the ^{14}N complex and at 1224 cm^{-1} for the ^{15}N complex.

Table 2. Selected Bond Distances (Å) in *trans*-$[Os^{VI}(tpy)(Cl)_2(NN(CH_2)_4O)](PF_6)_2$ (3), *cis*-$[Os^{V}(tpy)(Cl)(CH_3CN)(NN(CH_2)_4O)](PF_6)_2$ (5), *trans*-$[Os^{V}(tpy)(Cl)_2(NN(CH_2)_4CH_2)](PF_6)$ (6), $[Os^{IV}(tpm)(Cl)_2(N(H)N(CH_2)_4O)](PF_6)$ (7A), and $[Os^{V}(tpm)(Cl)_2(NN(C_2H_5)_2)](BF_4)$ (9b) According to the Labeling Schemes in Figures 1−3

trans-$[Os^{VI}(tpy)(Cl)_2(NN(CH_2)_4O)](PF_6)_2$ (**3**)			
Os(1)−Cl(1)	2.3193(22)	Os(1)−N(21)	2.004(7)
Os(1)−Cl(2)	2.3472(23)	Os(1)−N(31)	2.099(7)
Os(1)−N(1)	1.778(8)	N(1)−N(2)	1.234(12)
Os(1)−N(11)	2.086(7)		
cis-$[Os^{V}(tpy)(Cl)(CH_3CN)(NN(CH_2)_4O)](PF_6)_2$ (**5**) (A)			
Os(1)−Cl(1)	2.3639(25)	Os(1)−N(121)	1.971(9)
Os(1)−N(101)	1.915(7)	Os(1)−N(131)	2.093(8)
Os(1)−N(108)	2.053(9)	N(101)−N(102)	1.171(12)
Os(1)−N(111)	2.123(7)		
cis-$[Os^{V}(tpy)(Cl)(CH_3CN)(NN(CH_2)_4O)](PF_6)_2$ (**5**) (**B**)			
Os(2)−Cl(2)	2.3603(24)	Os(2)−N(231)	2.091(7)
Os(2)−N(201)	1.846(8)	Os(2)−N(208)	2.072(7)
Os(2)−N(221)	1.968(7)	N(201)−N(202)	1.266(11)
Os(2)−N(211)	2.085(8)		
trans-$[Os^{V}(tpy)(Cl)_2(NN(CH_2)_4CH_2)](PF_6)$ (**6**)			
Os(1)−Cl(1)	2.373(3)	Os(1)−N(21)	2.014(10)
Os(1)−Cl(2)	2.377(3)	Os(1)−N(31)	2.078(9)
Os(1)−N(1)	1.855(9)	N(1)−N(2)	1.243(15)
Os(1)−N(11)	2.089(9)		
$[Os^{IV}(tpm)(Cl)_2(N(H)N(CH_2)_4O)](PF_6)$ (**7a**)			
Os(1)−Cl(1)	2.3872(24)	Os(1)−N(21)	2.074(7)
Os(1)−Cl(2)	2.4036(22)	Os(1)−N(31)	2.064(8)
Os(1)−N(1)	1.904(8)	N(1)−N(2)	1.317(12)
Os(1)−N(11)	2.045(7)		
$[Os^{V}(tpm)(Cl)_2(NN(C_2H_5)_2)](BF_4)$ (**9b**)			
Os(1)−Cl(1)	2.3661(13)	Os(1)−N(21)	2.116(4)
Os(1)−Cl(2)	2.3718(12)	Os(1)−N(31)	2.059(4)
Os(1)−N(1)	1.855(4)	N(1)−N(2)	1.231(6)
Os(1)−N(11)	2.062(4)		

^{1}H NMR. The ^{1}H NMR spectrum of $[Os^{IV}(tpm)(Cl)_2(N(H)N(CH_2)_4O)](PF_6)$ in CD_3CN shows no sign of paramagnetic shifts confirming that the complex is a diamagnetic d^4 case. The aminoalkyl protons are not equivalent with resonances appearing in the range 3.32−3.98 ppm. The proton on the C(sp^3) bridgehead of the tpm ligand appears at 9.12 ppm, and the nine aromatic protons of the three pyrazolyl rings in the range 6.60−8.39 ppm. The complexes *cis*-$[Os^{IV}(tpy)(NCCH_3)(Cl)(NN(CH_2)_4O)](PF_6)$, *cis*-$[Os^{IV}(tpy)(NCCH_3)_2(NN(CH_2)_4O)](PF_6)_2$, and *trans*-$[Os^{VI}(tpy)(Cl)_2(NN(CH_2)_4O)](PF_6)_2$ are also diamagnetic by ^{1}H NMR spectroscopy. The tripplet aminoalkyl protons appear in the ranges of 1.08−1.14 ppm and 3.37−3.41 ppm. The 11 aromatic protons of tpy appear in the range of 7.97−8.63 ppm.

(14) (a) Coia, G. M.; Devenney, M.; White, P. S.; Meyer, T. J.; Wink, D. A. *Inorg. Chem.* **1997**, *36*, 2341. (b) Coia, G. M.; White, P. S.; Meyer, T. J.; Wink, D. A.; Keefer, L. K.; Davis, P. S. *J. Am. Chem. Soc.* **1994**, *116*, 3649.

(15) (a) Lumpkin, R. S.; Kober, E. M.; Worl, L. A.; Murtaza, Z.; Meyer, T. J. *J. Phys. Chem.*, **1990**, *94*, 239−243. (b) Pipes, D. W.; Bakir, M.; Vitols, S. E.; Hodgson, D. J.; Meyer, T. J. *J. Am. Chem. Soc.* **1990**, *112*, 5507. (c) Williams, D. S.; Meyer, T. J.; White, P. S. *J. Am. Chem. Soc.* **1995**, *117*, 823. (d) Pipes, D. W.; Meyer, T. J. *Inorg. Chem.* **1984**, *23*, 2466. (e) Kober, E. M.; Caspar, J. V.; Sullivan, B. P.; Meyer, T. J. *Inorg. Chem.* **1988**, *27*, 4587. (f) Megehee, E. G.; Meyer, T. J. *Inorg. Chem.* **1989**, *28*, 4084.

(16) Chatt, J.; Diamantis, A. A.; Heath, G. A.; Hooper, N. E.; Leigh, G. J. *J. Chem. Soc., Dalton Trans.* **1977**, 688.

Discussion

Our work demonstrates that rapid reactions occur between Os(VI) nitrido complexes and secondary amines. The net reaction between *trans*-$[Os^{VI}(tpy)(Cl)_2(N)]^+$ and morpholine as the example is shown in eq 4. Reactions between the nitrido complexes and primary and tertiary amines are currently under investigation.

$$2\ \textit{trans}\text{-}[Os^{VI}(tpy)(Cl)_2(N)]^+ + 2HN(CH_2)_4O \rightarrow \textit{trans}\text{-}[Os^{V}(tpy)(Cl)_2(NN(CH_2)_4O)]^+ + {}^1/_2\ \textit{trans,trans}\text{-}[(tpy)(Cl)_2Os^{II}(N_2)Os^{II}(Cl)_2(tpy)] + H_2N(CH_2)_4O^+ \quad (4)$$

The kinetic study gives insight into the mechanism by which the hydrazido complexes form. The electrochemical results reveal an extensive redox chemistry and access to Os(III) in solution and to the corresponding Os(IV), Os(V), and Os(VI) forms. Examples of all three oxidation states from Os(IV) to Os(VI) have been characterized by X-ray crystallography, and the structures allow some significant conclusions to be drawn concerning bonding and structure.[7]

Mechanism of Formation. The rate laws for the reactions between *trans*-$[Os^{VI}(tpy)(Cl)_2(N)]^+$ or $[Os^{VI}(tpm)(Cl)_2(N)]^+$ and morpholine ($HN(CH_2)_4O$) are first order in $Os^{VI}{\equiv}N^+$ and second order in $HN(CH_2)_4O$. A mechanism consistent with this rate law is shown in eqs 5−7.

$$[Os^{VI}(tpy)(Cl)_2(N)]^+ + HN(CH_2)_4O \underset{k_{-1}}{\overset{k_1}{\rightleftharpoons}} [Os^{IV}(tpy)(Cl)_2(N(H)N(CH_2)_4O)]^+ \quad (5)$$

$$[Os^{IV}(tpy)(Cl)_2(N(H)N(CH_2)_4O)]^+ + HN(CH_2)_4O \xrightarrow{k_2} [Os^{IV}(tpy)(Cl)_2(NN(CH_2)_4O)] + H_2N(CH_2)_4O^+ \quad (6)$$

$$[Os^{IV}(tpy)(Cl)_2(NNR_2)] + [Os^{VI}(tpy)(Cl)_2(N)]^+ \xrightarrow{\text{rapid}} [Os^{V}(tpy)(Cl)_2(NNR_2)]^+ + {}^1/_2\ \textit{trans,trans}\text{-}[(tpy)(Cl)_2Os^{II}(N_2)Os^{II}(tpy)(Cl)_2] \quad (7)$$

The key steps in this mechanism are the following: (1) initial formation of a protonated Os(IV) hydrazido intermediate; (2) deprotonation by a second morpholine molecule; (3) further oxidation to the Os(V) hydrazido product by $Os^{VI}{\equiv}N^+$. It is known from previous work that reduction of $Os^{VI}{\equiv}N^+$ to $Os^{V}{\equiv}N^0$ is followed by rapid N···N coupling.[3a]

There is no evidence for the buildup of the protonated intermediate in eq 5. This observation and the experimental rate law are consistent with a rapid preequilibrium and the mechanism in eqs 5−7 in the limit that $k_{-1} \gg k_2[HN(CH_2)_4O]$ with $k = k_2(k_1/k_{-1})$ and k = the experimental rate constant. The overall mechanism successfully accounts for the reaction stoichiometry and the appearance of the μ-N_2 complex as a coproduct.

The reaction labeled k_1 in eq 5 presumably occurs stepwise with adduct formation in the first step

$$[(tpy)(Cl)_2Os^{VI}{\equiv}N]^+ + HNR_2 \underset{k_{-i}}{\overset{k_i}{\rightleftharpoons}} \left[(tpy)(Cl)_2Os^{IV}{=}N{-}\overset{H}{\underset{R}{N}}{-}R\right]^+ \quad (8)$$

and intramolecular proton transfer in a second step since the proton has been shown to reside on N_α in $[Os^{IV}(tpm)(Cl)_2(N_\alpha(H)N_\alpha(CH_2)_4O)]^+$, Figure 3, eq 9.

$$\left[(tpy)(Cl)_2Os^{IV}{=}N_\alpha{-}N_\beta R_2H\right]^+ \underset{k_{-ii}}{\overset{k_{ii}}{\rightleftharpoons}} \left[(tpy)(Cl)_2Os^{IV}{=}N_\alpha{-}\overset{H}{N_\beta R_2}\right]^+ \quad (9)$$

The implied reversibility of eq 5 is a reflection of the relative instabilities of the protonated forms of the hydrazido complexes toward internal disproportionation by the k_{-1} step.[9a] It also suggests that these complexes, or their tertiary amine analogues,

Table 3. Selected Bond Angles (deg) in *trans*-$[Os^{VI}(tpy)(Cl)_2(NN(CH_2)_4O)](PF_6)_2$ (3), *cis*-$[Os^{V}(tpy)(Cl)(CH_3CN)(NN(CH_2)_4O)](PF_6)_2$ (5), *trans*-$[Os^{V}(tpy)(Cl)_2(NN(CH_2)_4CH_2)](PF_6)$ (6), $[Os^{IV}(tpm)(Cl)_2(N(H)N(CH_2)_4O)](PF_6)$ (7A), and $[Os^{V}(tpm)(Cl)_2(NN(C_2H_5)_2)](BF_4)$ (9b) According to the Labeling Schemes in Figures 1−3

trans-$[Os^{VI}(tpy)(Cl)_2(NN(CH_2)_4O)](PF_6)_2$ (**3**)			
Cl(1)−Os(1)-Cl(2)	168.16(9)	Cl(2)−Os(1)-N(31)	88.64(21)
Cl(1)−Os(1)-N(1)	99.08(23)	N(1)−Os(1)-N(11)	100.3(3)
Cl(1)−Os(1)-N(11)	87.77(20)	N(1)−Os(1)-N(21)	175.0(3)
Cl(1)−Os(1)-N(21)	85.56(20)	N(1)−Os(1)-N(31)	102.7(3)
Cl(1)−Os(1)-N(31)	89.61(21)	N(11)−Os(1)-N(21)	77.08(3)
Cl(2)−Os(1)-N(1)	92.72(23)	N(11)−Os(1)-N(31)	157.0(3)
Cl(2)−Os(1)-N(11)	82.61(19)	N(21)−Os(1)-N(31)	79.2(3)
Cl(2)−Os(1)-N(21)	88.64(20)	Os(1)−N(1)-N(2)	170.3(7)
cis-$[Os^{V}(tpy)(Cl)(CH_3CN)(NN(CH_2)_4O)](PF_6)_2$ (**5**) (**A**)			
Cl(1)−Os(1)-N(101)	178.37(22)	N(101)−Os(1)-N(131)	91.1(3)
Cl(1)−Os(1)-N(108)	87.69(25)	N(108)−Os(1)-N(111)	103.0(3)
Cl(1)−Os(1)-N(111)	88.11(21)	N108)-Os(1)−N(121)	174.9(3)
Cl(1)−Os(1)-N(121)	88.12(25)	N(108)−Os(1)-N(131)	79.3(3)
Cl(1)−Os(1)-N(131)	87.93(22)	N(111)−Os(1)-N(121)	79.8(3)
N(101)−Os(1)-N(108)	91.1(3)	N(111)−Os(1)-N(131)	159.1(3)
N(101)−Os(1)-N(111)	93.2(3)	N(121)−Os(1)-N(131)	79.6(3)
N(101)−Os(1)-N(121)	93.0(3)	Os(1)−N(101)-N(102)	148.9(8)
cis-$[Os^{V}(tpy)(Cl)(CH_3CN)(NN(CH_2)_4O)](PF_6)_2$ (**5**) (**B**)			
Cl(2)−Os(2)-N(201)	1.77.60(24)	N(201)−Os(2)-N(208)	93.5(3)
Cl(2)−Os(2)-N(221)	87.35(20)	N(221)−Os(2)-N(211)	80.2(3)
Cl(2)−Os(2)-N(211)	87.92(20)	N(221)−Os(2)-N(231)	80.4(3)
Cl(2)−Os(2)-N(231)	86.82(20)	N(221)−Os(2)-N(208)	173.9(3)
Cl(2)−Os(2)-N(208)	86.92(23)	N(211)−Os(2)-N(231)	160.1(3)
N(201)−Os(2)-N(221)	92.1(30)	N(211)−Os(2)-N(208)	97.6(3)
N(201)−Os(2)-N(211)	89.7(3)	N(231)−Os(2)-N(208)	101.2(3)
N(201)−Os(2)-N(231)	95.4(3)	Os(2)−N(101)-N(202)	148.9(7)
trans-$[Os^{V}(tpy)(Cl)_2(NN(CH_2)_4CH_2)](PF_6)$ (**6**)			
Cl(1)−Os(1)-Cl(2)	171.54(11)	Cl(2)−Os(1)-N(31)	90.8(3)
Cl(1)−Os(1)-N(1)	92.6(3)	N(1)−Os(1)-N(11)	100.9(4)
Cl(1)−Os(1)-N(11)	86.92(25)	N(1)−Os(1)-N(21)	178.8(4)
Cl(1)−Os(1)-N(21)	86.6(2)	N(1)−Os(1)-N(31)	102.7(4)
Cl(1)−Os(1)-N(31)	88.7(3)	N(11)−Os(1)-N(21)	78.2(4)
Cl(2)−Os(1)-N(1)	95.7(3)	N(11)−Os(1)-N(31)	156.1(4)
Cl(2)−Os(1)-N(11)	90.14(24)	N(21)−Os(1)-N(31)	78.2(4)
Cl(2)−Os(1)-N(21)	85.0(3)	Os(1)−N(1)-N(2)	157.2(9)
$[Os^{IV}(tpm)(Cl)_2(N(H)N(CH_2)_4O)](PF_6)$ (**7a**)			
Cl(1)−Os(1)-Cl(2)	92.12(8)	Cl(2)−Os(1)-N(31)	172.59(23)
Cl(1)−Os(1)-N(1)	96.45(24)	N(1)−Os(1)-N(11)	89.0(3)
Cl(1)−Os(1)-N(11)	173.75(22)	N(1)−Os(1)-N(21)	174.2(3)
Cl(1)−Os(1)-N(21)	89.10(22)	N(1)−Os(1)-N(31)	94.8(3)
Cl(1)−Os(1)-N(31)	90.43(22)	N(11)−Os(1)-N(21)	85.4(3)
Cl(2)−Os(1)-N(1)	91.80(25)	N(11)−Os(1)-N(31)	86.0(3)
Cl(2)−Os(1)-N(11)	90.82(21)	N(21)−Os(1)-N(31)	83.3(3)
Cl(2)−Os(1)-N(21)	89.78(21)	Os(1)−N(1)-N(2)	136.0(6)
$[Os^{V}(tpm)(Cl)_2(NN(C_2H_5)_2)](BF_4)$ (**9b**)			
Cl(1)−Os(1)-Cl(2)	91.17(5)	Cl(2)−Os(1)-N(31)	90.43(11)
Cl(1)−Os(1)-N(1)	96.89(13)	N(1)−Os(1)-N(11)	93.22(16)
Cl(1)−Os(1)-N(11)	90.50(12)	N(1)−Os(1)-N(21)	172.87(17)
Cl(1)−Os(1)-N(21)	89.05(11)	N(1)−Os(1)-N(31)	90.13(16)
Cl(1)−Os(1)-N(31)	172.70(11)	N(11)−Os(1)-N(21)	82.73(15)
Cl(2)−Os(1)-N(1)	93.41(13)	N(11)−Os(1)-N(31)	87.08(16)
Cl(2)−Os(1)-N(11)	172.92(11)	N(21)−Os(1)-N(31)	83.82(15)
Cl(2)−Os(1)-N(21)	90.42(11)	Os(1)−N(1)-N(2)	148.5(4)

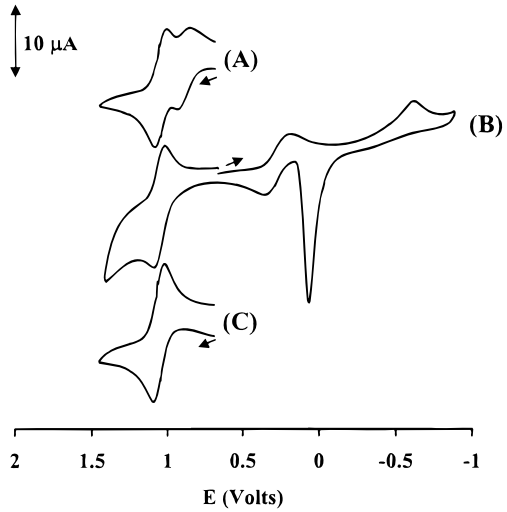

Figure 4. Cyclic voltammogram of a mixture of $[Os^{IV}(tpm)(Cl)_2(N(H)N(CH_2)_4O)](PF_6)$ and $[Os^{V}(tpm)(Cl)_2(NN(CH_2)_4O)](PF_6)$ in CH_3CN 0.1 M in TBAH versus SSCE: (A) Os(VI/V) couple of $[Os^{V}(tpm)(Cl)_2(NN(CH_2)_4O)](PF_6)$ and Os(V/IV) couple of $[Os^{IV}(tpm)(Cl)_2(N(H)N(CH_2)_4O)](PF_6)$; (B) Os(VI/V), Os(V/IV) and Os(IV/III) couples of $[Os^{V}(tpm)(Cl)_2(NN(CH_2)_4O)](PF_6)$; (C) Os(VI/V) couple of $[Os^{V}(tpm)(Cl)_2(NN(CH_2)_4O)](PF_6)$ remaining after the addition of 2,2′-bipyridine to the solution mixture containing $[Os^{IV}(tpm)(Cl)_2(N(H)N(CH_2)_4O)](PF_6)$ and $[Os^{V}(tpm)(Cl)_2(NN(CH_2)_4O)](PF_6)$.

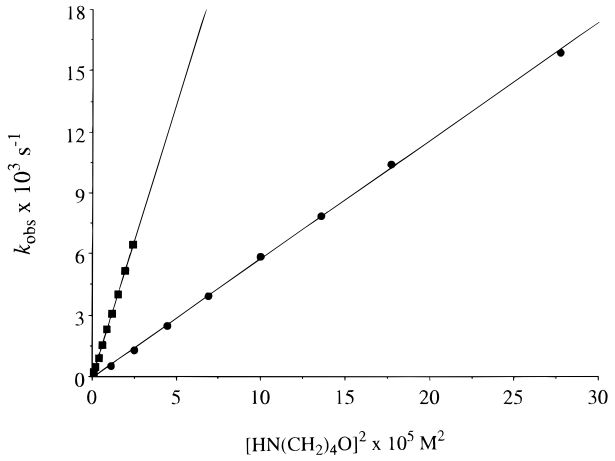

Figure 5. Plot of k_{obs} versus $[HN(CH_2)_4O]^2$ for the formation of *trans*-$[Os^{V}(tpy)(Cl)_2(NN(CH_2)_4O)](PF_6)$ (●) and of $[Os^{V}(tpm)(Cl)_2(NN(CH_2)_4O)](PF_6)$ (■) in CH_3CN at 25.0 ± 0.1 °C.

should have an $Os^{VI}{\equiv}N$-like reactivity, a possibility that is currently under investigation.

The initial redox step in eq 8 is a concerted two-electron, atom transfer. One-electron reduction is a common reaction for $Os^{VI}{\equiv}N^+$, and when it occurs, the μ-N_2 complex is the product.[2,3,5,6] There is ample literature precedence for atom transfer including reactions between $Os^{VI}{\equiv}N^+$ and PR_3 to give stable Os^{IV} phosphoraniminato products.[2] The reaction betwwen *trans*-$[Os^{VI}(tpy)(Cl)_2N]^+$ and PPh_3, eq 10, occurs with $k = (1.36 \pm 0.08) \times 10^4$ M^{-1} s^{-1} in CH_3CN at 25 °C.

$$[Os^{VI}(tpy)(Cl)_2(N)]^+ + PPh_3 \rightarrow [Os^{IV}(tpy)(Cl)_2(NPPh_3)]^+ \quad (10)$$

N-atom transfer is a common reaction for nitrido complexes with known examples for nitrido complexes of Mo(III),[19] Cu(I),[20] Cr(V),[21] Mn(V),[22] Re(V),[23] Ru(VI), and Os(VI).[24] In the reactions between $Os^{VI}{\equiv}N^+$ and the secondary amines, two electrons are transferred to Os(VI) accompanied by N^{3-} transfer to the amine. Given the hydrazido product, in a formal sense, there is net transfer of N^-. Atom transfer has also been invoked in reactions between $Os^{VI}{\equiv}N^+$ and N_3^- in CH_3CN[3] and between $Os^{VI}{\equiv}N^+$ and N_3^- in the presence of CS_2 in acetone.[17]

$$[Os^{VI}(tpm)(Cl)_2(N)]^+ + N_3^- \rightarrow [Os^{II}(tpm)(Cl)_2(N_2)] + N_2 \quad (11)$$

$$N_3^- + CS_2 \rightleftharpoons CS_2N_3^- \quad (12a)$$

$$[Os^{VI}(tpy)(Cl)_2(N)]^+ + CS_2N_3^- \rightarrow [Os^{II}(tpy)(Cl)_2(NS)]^+ + SCN^- + N_2 \quad (12b)$$

In these reactions, atom transfer is accompanied by profound changes in internal electronic distribution with a net conversion of Os(VI) to Os(II). In the reaction with N^{3-}, attack on the N atom of $Os^{VI}{\equiv}N^+$ occurs by N^- transfer with N_2 the leaving group. With CS_2 added, the cyclic adduct $CS_2N_3^-$ forms, and N^- is transferred with NCS^- and N_2 as the leaving groups.[3d] Similarly, O-atom transfer to $Os^{VI}{\equiv}N^+$ by $ONMe_3$ leads to a four-electron change at Os and a six-electron change at N (from −III to +III).[18]

$$trans\text{-}[Os^{VI}(tpy)(Cl)_2(N)]^+ + ONMe_3 \rightarrow trans\text{-}[Os^{II}(tpy)(Cl)_2(NO)]^+ + NMe_3 \quad (13)$$

Significant electronic structural changes accompany N-atom (or N^-) transfer. Defining the *z* axis to fall along the Os−N bond in $Os^{VI}{\equiv}N^+$, the d-electronic configuration is $d\pi_{xy}^2$, $d\pi^*_{xz}{}^0$, $d\pi^*_{yz}{}^0$. There is considerable antibonding character in the nominally $d\pi_{xz}$ and $d\pi_{yz}$ orbitals because of extensive $d\pi$-$(Os^{VI})-2p_\pi(N)$ mixing.[9,25] These orbitals are available for an initial electronic interaction with the lone pair in $sp^3(N)$ on the amine. This is followed by transfer of an electron pair to $d\pi^*$, a change in hybridization at N_α to sp^2 from sp by mixing with $2p_\pi(N)$, and formation of the N−N bond by overlap between $sp^3(N_\alpha)$ and $sp^2(N_\alpha)$. The electronic structures of the final deprotonated Os(IV) products are discussed in the next section.

In dry CH_3CN, the rate-determining step in the mechanism in eqs 5−7 is deprotonation. This might not be the case in water since the protonated adducts are relatively acidic with $pK_a = 3.20 \pm 0.04$ for *trans*-$[Os^{IV}(tpy)(Cl)_2(N(H)N(CH_2)_4O)]^+$ in 1:1 (v/v) CH_3CN:H_2O. However, work currently in progress shows

(17) (a) El-Samanody, El.-S.; Demadis, K. D.; Gallagher, L. A.; Meyer, T. J.; White, P. S. *Inorg. Chem.* **1999**, *38*, 3329. (b) Demadis, K. D.; Meyer, T. J.; White, P. S. *Inorg. Chem.* **1998**, *37*, 3610.
(18) Williams, D. S.; Meyer, T. J.; White, P. S. *J. Am. Chem. Soc.* **1995**, *117*, 823.
(19) Cummins, C. C. *Prog. Inorg. Chem.* **1998**, *47*, 685.
(20) Ando, T.; Minakata, S.; Ryu, I.; Komatsu, M. *Tetrahedron Lett.* **1998**, *39* (3−4), 309.
(21) Neely, F. L.; Bottomley, L. A. *Inorg. Chem.* **1997**, *36*, 5432.
(22) (a) DuBois, J.; Tomooka, C. S.; Hong, J.; Carreira, E. M. *Acc. Chem. Res.* **1997**, *30* (9), 364. (b) Groves, J. T.; Lee, J. B.; Marla, S. S. *J. Am. Chem. Soc.* **1997**, *119*, 6269. (g) Chang, C. J.; Low, D. W.; Gray, H. B. *Inorg. Chem.* **1997**, *36*, 270.
(23) Tong, C.; Jones, J. A.; Bottomley, L. A. *Inorg. Chim. Acta* **1996**, *251* (1−2), 105.
(24) (a) Sellmann, D.; Wemple, M. W.; Donaubauer, W.; Heinemann, F. W. *Inorg. Chem.* **1997**, *36*, 1397. (b) Chan, P. M.; Yu, W. Y.; Che, C. M.; Cheung, K. K. *J. Chem. Soc., Dalton Trans.* **1998**, 3183.
(25) Kahlal, S.; Saillard, J.-Y.; Hamom, J.-R.; Manzur, C.; Carrillo, D. *J. Chem. Soc., Dalton Trans.* **1998**, 1229.

Table 4. UV−Visible and Electrochemical Data for Salts **3**−**9** in CH_3CN

Salts	λ_{max}, nm ($10^{-3}\epsilon$, M^{-1} cm^{-1})	$E_{1/2}$ vs SSCE[a]		
		Os(VI/V)	Os(V/IV)	Os(IV/III)
trans-$[Os^{VI}(tpy)(Cl)_2(NN(CH_2)_4O)](PF_6)_2$ (**3**)	790 (0.13), 586 (0.43), 470 (2.39), 330 (21.2), 288 (25.4), 252 (35.7), 208 (44.7)	+0.98	0.00	−0.79
trans-$[Os^{V}(tpy)(Cl)_2(NN(CH_2)_4O)](PF_6)$ (**4**)	879 (0.35), 668 (1.17), 565 (1.80), 420 (4.02), 398 (4.28), 312 (22.8), 264 (30.2), 230 (33.9), 194 (36.7)			
cis-$[Os^{V}(tpy)(Cl)(CH_3CN)(NN(CH_2)_4O)](PF_6)_2$ (**5**)	656 (0.27), 532 (0.99), 480 (1.77), 428 (2.86), 316 (19.3), 284 (21.9), 242 (27.4), 218 (28.7)	+1.30	+0.42	−0.22
trans-$[Os^{V}(tpy)(Cl)_2(NN(CH_2)_4CH_2)](PF_6)$ (**6**)	658 (0.97), 424 (3.92), 402 (4.02), 314 (20.2), 258 (26.5), 234 (29.3), 212 (26.3)	+0.90	−0.05	−0.75
$[Os^{V}(tpm)(Cl)_2(NN(CH_2)_4O)](PF_6)$ (**7a**)	676 (0.10), 400 (16.6), 286 (27.0), 218 (17.2)	+1.05	+0.27	−0.62[b]
$[Os^{V}(tpm)(Cl)_2(NN(CH_2)_4CH_2)](PF_6)$ (**8a**)	610 (0.16), 382 (10.9), 326 (6.19), 228 (21.0), 214 (16.7)	+0.95	0.05	−0.77[b] −0.05[c]
$[Os^{V}(tpm)(Cl)_2(NN(C_2H_5)_2)](PF_6)$ (**9a**)	672 (0.23), 403 (13.5), 337 (7.58), 285 (25.2), 221 (20.5), 205 (23.7)	+0.92	+0.03	−0.77[b] −0.08
$[Os^{IV}(tpy)(Cl)_2(N(H)N(CH_2)_4O)](PF_6)$	975 (0.72), 859 (0.64), 572 (1.44), 454 (7.06), 280 (19.0), 272 (18.9), 250 (16.9)	+0.98	+0.84[d]	

[a] Volts vs SSCE in 0.1 M TBAH/CH_3CN. [b] E_{pc} (Os(IV) → Os(III)). [c] E_{pa} (Os(III) → Os(IV)). [d] $Os^{V/IV}$−N(H)N$(CH_2)_4$O.

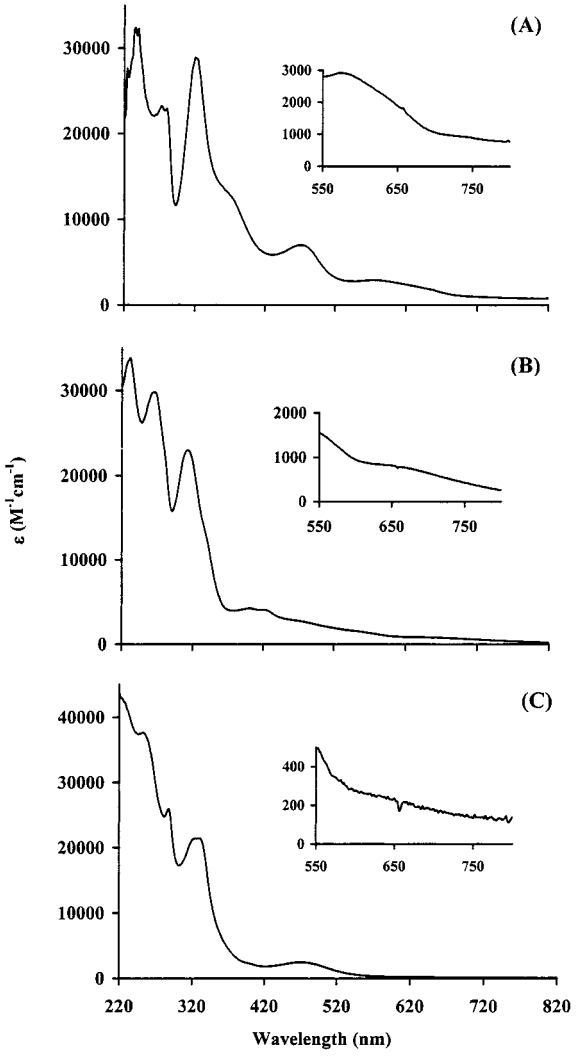

Figure 6. Absorption spectra in CH_3CN: (A) *trans*-$[Os^{IV}(tpy)(Cl)_2(N(H)N(CH_2)_4O)](PF_6)$; (B) *trans*-$[Os^{V}(tpy)(Cl)_2(NN(CH_2)_4O)](PF_6)$; (C) *trans*-$[Os^{VI}(tpy)(Cl)_2(NN(CH_2)_4O)](PF_6)_2$.

that in the electrochemical oxidation of *trans*-$[Os^{IV}(tpy)(Cl)_2(N(H)N(CH_2)_4O)]^+$ proton loss precedes electron transfer and is relatively slow.[13b]

Deprotonation plays an important role. It stabilizes Os(IV) toward the internal hydrazido disproportionation k_{-1} step in eq 5. It also stabilizes the Os(V) oxidation state as evidenced by the decrease Os(V/IV) potential from 0.72 V (versus SSCE in CH_3CN) for the Os(V/IV) couple for the $[Os^{IV}(tpm)(Cl)_2(N(H)N(CH_2)_4O)]^{+/0}$ to 0.27 V for the $[Os^{V}(tpm)(Cl)_2(NN(CH_2)_4O)]^{+/0}$ couple.

Table 5. UV−Visible and near-IR Band Assignments for Os(IV), Os(V), and Os(VI) hydrazido Complexes in CH_3CN

Complex	Band energy, nm (cm^{-1}) ($10^{-3}\epsilon$, M^{-1} cm^{-1})	Assgnt
trans-$[Os^{IV}(tpy)(Cl)_2(N(H)N(CH_2)_4O)]^{+}$ [a]	975 (0.72)	$d\pi_2 \rightarrow d\pi^*$
	859 (0.64)	$d\pi_1 \rightarrow d\pi^*$
	572 (1.44)	MLCT
	454 (7.06)	MLCT
$[Os^{IV}(tpy)(bpy)(N(H)N(CH_2)_4O)]^{3+}$ [b]	976 (2.18)	$d\pi_2 \rightarrow d\pi^*$
	868 (1.42)	$d\pi_1 \rightarrow d\pi^*$
	438 (21.9)	MLCT
	362 (15.5)	MLCT
trans-$[Os^{IV}(tpy)(Cl)(CH_3CN)(NN(CH_2)_4O)]^{2+}$	660 (2.82)	$d\pi_1^* \rightarrow d\pi_2^*$
	580 (3.43)	$d\pi_n \rightarrow d\pi_2^*$
	470 (3.79)	MLCT
	402 (4.99)	MLCT
$[Os^{IV}(tpy)(bpy)(NN(CH_2)_4O)]^{2+}$	620 (4.40)	$d\pi_1^* \rightarrow d\pi_2^*$
	522 (5.83)	$d\pi_n \rightarrow d\pi_2^*$
	442 (9.24)	MLCT
	394 (12.0)	MLCT
trans-$[Os^{V}(tpy)(Cl)_2(NN(CH_2)_4O)]^{+}$	879 (0.35)	$d\pi_n \rightarrow d\pi_1^*$
	668 (1.17)	$d\pi_1^* \rightarrow d\pi_2^*$
	565 (1.80)	$d\pi_n \rightarrow d\pi_2^*$
	420 (4.02)	MLCT
	398 (4.28)	LMCT
$[Os^{V}(tpy)(bpy)(NN(CH_2)_4O)^{3+}$	807 (0.30)	$d\pi_n \rightarrow d\pi_1^*$
	570 (0.95)	$d\pi_1^* \rightarrow d\pi_2^*$
	505 (1.69)	$d\pi_n \rightarrow d\pi_2^*$
	484 (1.98)	MLCT
	430 (2.47)	LMCT
trans-$[Os^{VI}(tpy)(Cl)_2(NN(CH_2)_4O)]^{2+}$	790 (0.13)	$d\pi_n \rightarrow d\pi_1^*$
	586 (0.43)	$d\pi_n \rightarrow d\pi_2^*$
	470 (2.39)	LMCT

[a] In 1:1 (v/v) CH_3CN-H_2O in μ = 0.1 M HNO_3. [b] In 6.0 M HCl.

The decrease in potential triggers oxidation by unreacted $Os^{VI}\equiv N^+$, eq 14, which leads to the μ-N_2 complex by rapid,

$$[Os^{VI}(tpy)(Cl)_2(N)]^+ + [Os^{IV}(tpy)(Cl)_2(NN(CH_2)_4O)]^+ \rightarrow [Os^{V}(tpy)(Cl)_2(N)] + [Os^{V}(tpy)(Cl)_2(NN(CH_2)_4O)]^+ \quad (14)$$

following $Os^{V}N\cdots NOs^{V}$ coupling. At close to stoichiometric conditions for reaction 4, there is insufficient base to complete

the net reaction, and deprotonated Os(IV) builds up as a coproduct in solution. By carrying out the reaction under these conditions, we were able to isolate $[Os^{IV}(tpm)(Cl)_2(N(H)N(CH_2)_4O)]^+$ and characterize it by X-ray crystallography.

Redox Properties. The cyclic voltammetry results provide evidence for chemically reversible Os(VI/V), Os(V/IV), and Os(IV/III) couples.[5] Oxidation of *trans*-$[Os^V(tpy)(Cl)_2(NN(CH_2)_4O)]^+$ to *trans*-$[Os^{VI}(tpy)(Cl)_2(NN(CH_2)_4O)]^{2+}$ and reduction from *trans*-$[Os^{VI}(tpy)(Cl)_2(NN(CH_2)_4O)]^{2+}$ to *trans*-$[Os^V(tpy)(Cl)_2(NN(CH_2)_4O)]^+$ both occur with $n = 1$ as shown by coulometry. Reduction of *trans*-$[Os^V(tpy)(Cl)_2(NN(CH_2)_4O)]^+$ to *trans*-$[Os^{IV}(tpy)(Cl)_2(NN(CH_2)_4O)]^+$ is reversible on the cyclic voltammetry time scale, but reduction on the coulometric time scale is accompanied by isomerization and solvolysis to give *cis*-$[Os^{IV}(tpy)(Cl)(NCCH_3)(NN(CH_2)_4O)]^+$. This chemistry will be discussed in a future paper.[13]

Oxidation of $[Os^V(tpm)(Cl)_2(NN(CH_2)_4O)]^+$ to Os(VI) and reduction to Os(IV) are also reversible and occur with $n = 1$. Reduction to Os(III) past $E_{1/2} = -0.31$ V is accompanied by adsorption/precipitation on the electrode. This results in a desorption spike for the reverse, Os(III) → Os(IV) wave in the voltammograms (Figure 4B). Peak currents for the Os(V/IV) wave are smaller than those for the Os(VI/V) and Os(IV/III) waves (Figure 4B). This may be a consequence of surface coating during the voltammetric scans. When the electrode was polished between scans, the electroactivity for the Os(V/IV) wave was enhanced.

$E_{1/2}$ values depend on the ancillary ligand and the secondary amine (Table 4). For the Os(VI/V) couples, $E_{1/2}$ values for the morpholine adducts are 80−100 mV higher than for the piperidine adducts. $E_{1/2}$ values for the tpm complexes are 60−80 mV higher than for the tpy complexes. Small variations are also observed in the $E_{1/2}$ values for the Os(V/IV) and Os(IV/III) couples.

Structure and Bonding. Bond distance and angle information for five Os(V) hydrazido complexes are summarized in Tables 2 and 3. These complexes appear to be the first examples of transition metal d^3 hydrazido complexes that have been structurally characterized.[5−7,25]

There are common features in the structures. Os−N bond lengths (1.846(8)−1.915(7) Å) are significantly shorter than for typical Os−N single bonds (2.039(9)−2.123(7) Å). In other transition metal hydrazido complexes, the range in M−N bond distances is from 1.512(2) to 1.565(6) Å for the first row transition metals and from 1.570(7) to 1.830(4) Å for the second and third rows.[26,27]

The N−N bond of the hydrazido ligand is relatively short (1.231(6)−1.321(12) Å) consistent with a N−N double bond. The exception is the N−N bond in molecule A in the structure of *cis*-$[Os^V(tpy)(Cl)(NCCH_3)(NN(CH_2)_4O)](PF_6)_2$ which is even shorter at 1.171(12) Å. The range in N−N distances in other transition metal hydrazido complexes is from 1.21(2) Å in the W(II) d^4 complex $[W(NNMe_2)(CO)_3(dppe)]$ (dppe = 1,2-bis(diphenylphosphino)ethane)[28] to 1.42(6) Å) in the W(IV) d^2 complex $[W(NNCH_2CH_2CH_2)Br(dtpe)]^+$ (dtpe = 1,2-bis(di-*p*-tolylphosphino)ethane).[29]

In the known Os hydrazido complexes,[13,14] the Os−N−N angle varies from 129.3(7)° in d^4 Os(IV) *cis*-$[Os^{IV}(tpy)(Cl)(NCCH_3)(NN(CH_2)_4O)]^+$ to 170.3(7)° in d^2 Os(VI) *trans*-$[Os^{VI}(tpy)(Cl)_2(NN(CH_2)_4O)]^{2+}$. The range of M−N−N angles in other transition metal hydrazido examples is from 131.2(10)° for Re(VI) d^2 $[Re(NNHPh)(NNPh)(Br)_2(PPh_3)_2]$[30] to 180° for d^1 V(IV) $[V(C_5H_5)_2(NN(SiMe_3)_2)]$[31] and for d^4 Fe(IV) [Fe(tcpp)(NNC$_9$H$_{18}$)] (H_2tcpp = *meso*-5,10,15,20-tetra-*p*-chlorophenylporphyrin)].[32]

In comparison the Os(V) hydrazido structures in Tables 2 and 3, there are both notable similarities and notable differences. The structures of *trans*-$[Os^V(tpy)(Cl)_2(NN(CH_2)_4CH_2)]^+$ and $[Os^V(tpm)(Cl)_2(NN(CH_2CH_3)_2]^+$ are nearly identical in terms of the Os-hydrazido interaction even though the amine added, the coordination geometry, and the ancillary ligands are different. Similarly, in *trans*-$[Os^V(tpy)(Cl)_2(NN(CH_2)_4O)]^+$ and *trans*-$[Os^V(tpy)(Cl)_2(NN(CH_2)_4CH_2)]^+$, Os−N bond lengths and Os−N−N angles are nearly the same. Although they are formed from different amines, they share a common coordination geometry with the center N atom of the tpy ligand trans to the hydrazido ligand.

There are significant differences between the structures of cations A and B in the cocrystal of *cis*-$[Os^V(tpy)(Cl)(NCCH_3)(NN(CH_2)_4O)](PF_6)_2$. In A, the Os−N bond length (1.915(7) Å) is 0.069 Å longer than that in B which is consistent with other Os(V) hydrazido complexes. The N−N bond length in A is in the range for a N−N double bond. It is 0.095 Å longer in B. Other molecular dimensions are consistent with Os(V) hydrazido complexes. The Os−N−N bond angles are the same, which is significant since this angle is a sensitive probe of oxidation state at the metal, see below.[25] The origin of these structural differences is not understood.

Bonding in transition metal hydrazido complexes has been discussed in a recent review.[25] In the treatment of the hydrazido ligand as a dianion, NNR_2^{2-}, the Os−N$_\alpha$-N$_\beta$R$_2$ electronic interaction results in three filled molecular orbitals available for bonding to the metal. They are σ_N, π_N (an orbital derived largely from a 2pπ lone pair on N$_\alpha$), and π^*_{NN}. The π_{NN} orbital is not significantly involved in bonding with the metal and retains its multiple bond character as long as the hybridization at both N$_\alpha$ and N$_\beta$ is sp^2.

A schematic MO diagram for the d^4 hydrazido complexes derived from ref 25 is shown in Scheme 1. It can be used to explain the variations in important bond angles and distances between oxidation states that appear in the data in Tables 2 and 3.

In *trans*-$[Os^{VI}(tpy)(Cl)_2(NN(CH_2)_4O)]^{2+}$, the short Os−N bond (1.778(8) Å) and large Os−N−N angle (170.3(7)°) are both consistent with this bonding scheme. The hydrazido ligand acts as a six-electron donor with electron pair donation from σ_N, π_N, and π^*_{N-N}.

Upon reduction to d^3 Os(V), an electron is added to dπ_1* which is largely dπ(Os) but mixed with σ_N. This decreases the Os−N bond order to $2^1/_2$ and increases the Os−N bond length. It also decreases the Os−N−N angle in order to decrease electron−electron repulsion.

Addition of a second electron to give d^4 Os(IV), as in *cis*-$[Os^{IV}(tpy)(Cl)(NCCH_3)(NN(CH_2)_4O)]^+$, also occurs at d$\pi_1$* as shown by the diamagnetism of the product. This results in a

(26) Pipes, D. W.; Bakir, M.; Vitols, S. E.; Hodgson, D. J.; Meyer, T. J. *J. Am. Chem. Soc.* **1990**, *112*, 5507.
(27) Nugent, W. A.; Mayer, J. M. *Metal Ligand Multiple Bonds*; John Wiley & Sons: New York, 1988.
(28) Arndtsen, B. A.; Schoch, T. K.; McElwee-White, L. *J. Am. Chem. Soc.* **1992**, *114*, 7041.
(29) Bakar, M. A.; Hughes, D. L.; Leigh, G. L. *J. Chem. Soc., Dalton Trans.* **1988**, 2525.
(30) Dilworth, J. R.; Harrison, S. A.; Walton, D. R. M.; Schweda, E. *Inorg. Chem.* **1985**, *24*, 2594.
(31) Veith, M. *Angew. Chem., Int. Ed. Engl.* **1976**, *15*, 387.
(32) Komori, K.; Komada, T.; Jin, D.-M.; Takahashi, T.; Uchida, Y.; Hidai, M. *Chem. Lett.* **1983**, 465.

Scheme 1. Schematic Orbital Energy Level Diagram for the Hydrazido Complexes Showing the Electronic Configuration of Os(IV), from Ref 25

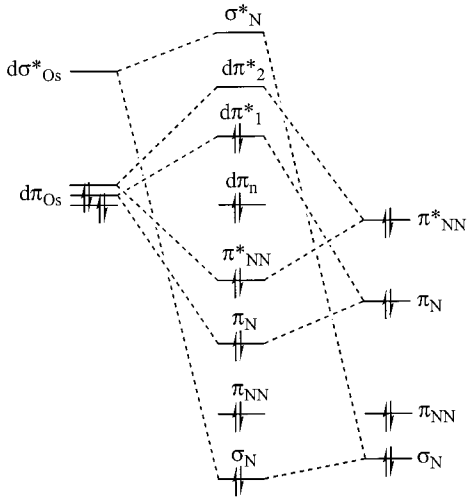

Scheme 2. Effect of Protonation at N_α on the Scheme 1

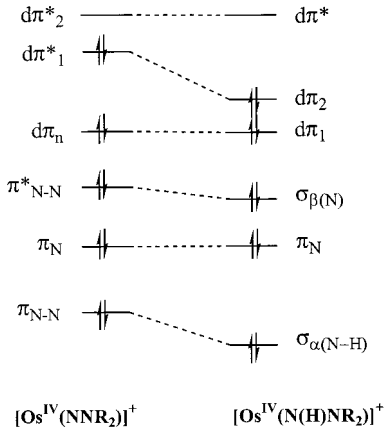

further decrease in Os−N bond order to 2 and further decreases ∠Os−N−N to reduce electron−electron repulsion.

From cyclic voltammetry and coulometry measurements, the d^5 Os(III) forms of *cis*-$[Os^{III}(tpy)(Cl)_2(NN(CH_2)_4O)]^-$ or $[Os^{III}(tpm)(Cl)_2(NN(CH_2)_4O)]^-$ are accessible in solution. We are currently attempting to isolate crystals suitable for X-ray analysis. On the basis of the bonding model, it is possible to predict an even longer Os−N bond and an Os−N−N angle nearer to 120° in these structures.

As mentioned above, protonation at N_α destabilizes Os(IV) toward internal disproportionation and increases the Os(V/IV) reduction potential. The orbital consequences of protonation are shown qualitatively in the correlation diagram in Scheme 2. The $2p_\pi(N_\alpha)$ and $2p_\pi(N_\beta)$ orbitals used to construct π_{NN} and π^*_{NN} are mixed with $2s(N_\alpha)$ and $2s(N_\beta)$ to form sp^2 orbitals at N_α-($\sigma_\alpha(N)$) and $N_\beta(\sigma_\beta(N))$. $\sigma_\alpha(N)$ is protonated and becomes σ_α-(N−H), and $\sigma_\beta(N)$ becomes a lone pair on N_β. This breaks up the N−N double bond and the $d\pi_1^*-\pi^*_{NN}$ interaction. This results in a loss of antibonding character in $d\pi_1^*$ which becomes $d\pi_2$.

Electronic Spectra. The energy level diagrams in Schemes 1 and 2 provide a basis for assigning the visible and near-IR spectra for the Os(IV), Os(V), and Os(VI) hydrazido complexes. Band assignments are tabulated in Table 5.

In the spectrum of the protonated form *trans*-$[Os^{IV}(tpy)(Cl)_2(N(H)N(CH_2)_4O)]^+$ (0.1 M in HNO_3 in 1:1 (v/v) $CH_3CN:H_2O$, at pH = 1), interconfigurational (IC), $d\pi \rightarrow d\pi$ bands appear at 859 nm ($d\pi_1 \rightarrow d\pi^*$) and 975 nm ($d\pi_2 \rightarrow d\pi^*$) where the assignment are based in Scheme 2. Metal-to-ligand charge transfer (MLCT) bands, $d\pi \rightarrow \pi^*$(tpy), appear at 454 and 572 nm. Analogous bands are observed for $[Os^{IV}(tpy)(bpy)(N(H)N(CH_2)_4O)]^{3+}$ in 6.0 M HCl with $d\pi_n \rightarrow d\pi^*$ appearing at 868 nm, $d\pi_2 \rightarrow d\pi^*$ at 976 nm, and MLCT bands at 362 and 438 nm.

On the basis of the energy level diagram in Scheme 1 for the deprotonated complex *cis*-$[Os^{IV}(tpy)(Cl)(CH_3CN)(NN(CH_2)_4O)]^+$ in CH_3CN, $d\pi_n \rightarrow d\pi_2^*$ appears at 580 nm, $d\pi_1^* \rightarrow d\pi_2^*$ appears at 660 nm, and MLCT bands appear at 402 and 470 nm. Analogous bands are observed for $[Os^{IV}(tpy)(bpy)(NN(CH_2)_4O)]^{2+}$ in CH_3CN with $d\pi_n \rightarrow d\pi_2^*$ appearing at 522 nm, $d\pi_1^* \rightarrow d\pi_2^*$ at 620 nm, and MLCT bands at 394 and 442 nm. The MLCT bands of *cis*-$[Os^{IV}(tpy)(Cl)(CH_3CN)(NN(CH_2)_4O)]^+$ appear at lower energy than those for $[Os^{IV}(tpy)(bpy)(NN(CH_2)_4O)]^{2+}$, which is consistent with the decrease in $E_{1/2}$(Os(V/IV)) from 0.67 to 0.42 V (in CH_3CN, versus SSCE).

In an earlier manuscript, it was suggested that the proper orbital ordering scheme for $[Os^{IV}(tpy)(bpy)(NN(CH_2)_4O)]^{2+}$ was $\pi_N < d\pi_n < d\pi_1^* < d\pi_2^* < \pi^*_{N-N}$ rather than the ordering in Scheme 1 which places π^*_{N-N} below $d\pi_n$.[14a] With this interpretation, the ground-state $d\pi$ electronic configuration would be $d\pi^6$ and the complexes viewed as Os(II) bound to isodiazene ligands rather than Os(IV) complexes bound to hydrazido ligands. Visible MLCT bands were assigned to $d\pi$-(Os^{II}) $\rightarrow \pi^*$(bpy), π^*(tpy) transitions rather than to the $d\pi$-(Os^{IV}) $\rightarrow \pi^*$(bpy), π^*(tpy) transition.

The observation of IC bands for these complexes supports the Os(IV) assignment and the ordering in Schemes 1 and 2. The MLCT assignments are reasonable on energy grounds. For example, for *trans*-$[Os^{II}(tpy)(Cl)_2(py)]$,[17] λ_{max} occurs at 592 nm with $E_{1/2}(Os^{III}/Os^{II}) = 0.12$ V (versus SSCE in CH_3CN) compared to λ_{max} at 454 nm and $E_{1/2}(Os^{V}/Os^{IV}) = 0.00$ V for *trans*-$[Os^{IV}(tpy)(Cl)_2(N(H)N(CH_2)_4O)]^+$. In this comparison, π^*_1(tpy) is the common acceptor level. The $E_{1/2}$ values for the Os^V/Os^{IV} couple show that the $d\pi-\pi^*$(tpy) energy gap is comparable to those typically found for MLCT transitions involving Os(II).[17] The molar absorptivities are lower than for typical Os(II) MLCT absorptions consistent with lower $d\pi$(Os-(IV) $\rightarrow \pi^*$(tpy)) overlap as expected for the lower oxidation state.

On the basis of orbital diagram in Scheme 1, oxidation from Os(IV) to Os(V) removes an electron from $d\pi_1^*$, and three $d\pi \rightarrow d\pi$ transitions are predicted to occur in the resulting $d\pi_n^2\, d\pi_1^{*1}$ configuration. Interconfigurational bands for *trans*-$[Os^{V}(tpy)(Cl)_2(NN(CH_2)_4O)]^+$ in CH_3CN appear at 565 nm ($d\pi_n \rightarrow d\pi_2^*$), 668 nm, and 879 nm. The latter two arise from the transitions $d\pi_1^* \rightarrow d\pi_2^*$ and $d\pi_n \rightarrow d\pi_1^*$; the order is not known. Additional, intense bands appear at 420 and 398 nm which appear to be $\pi^*_{NN} \rightarrow d\pi^*$, ligand-to-metal charge transfer (LMCT) bands. For $[Os^{V}(tpy)(bpy)(NN(CH_2)_4O)]^{3+}$ in CH_3CN, IC bands appear at 505 nm ($d\pi_n \rightarrow d\pi_2^*$), 570 nm, and 807 nm and LMCT bands at 484 and 430 nm. The lower energy for this transition compared to *trans*-$[Os^{V}(tpy)(Cl)_2(NN(CH_2)_4O)]^+$ is consistent with the increase in $E_{1/2}$(Os(V/IV)) from 0.00 to 0.67 V.

Further one-electron oxidation to Os(VI) removes the remaining $d\pi_1^*$ electron. In the spectrum of *trans*-$[Os^{VI}(tpy)(Cl)_2(NN(CH_2)_4O)]^{2+}$ in CH_3CN, $d\pi_n \rightarrow d\pi_2^*$ appears at 586 nm and $d\pi_n \rightarrow d\pi_1^*$ at 790 nm. A LMCT band appears at 470 nm which is red-shifted compared to Os(V) qualitatively consistent with

the increase in potential for the Os(VI/V) couple compared to the Os(V/IV) couple.

Acknowledgments are made to the National Science Foundation under Grant No. CHE-9503738 and the Department of Energy under Grant No. LM 19X-SX 092C for supporting this research. E.-S. E.-S. wishes to thank the Egyptian Government for the Data Collection Grant.

Supporting Information Available: Text giving experimental procedures for the preparation and characterization of the compounds, tables containing crystal data, atomic coordinates, isotropic thermal parameters, and bond distances and angles, and figures packing diagrams. This material is available free of charge via the Internet at http://pubs.acs.org.

IC000058E